




**Polarization-based cyclic weak value metrology for angular-velocity measurement**Zi-Rui Zhong , Yue Chen, Wei-Jun Tan, Xiang-Ming Hu , and Qing-Lin Wu <sup>\*</sup>*Department of Physics, Central China Normal University, Wuhan 430079, China  
and China Key Laboratory of Quark & Lepton Physics (MOE) and Institute of Particle Physics,  
Central China Normal University, Wuhan 430079, China*

(Received 3 November 2023; accepted 18 March 2024; published 1 April 2024)

Weak measurement has been proven to amplify the detection of changes in meters while discarding most photons due to the low probability of postselection. Previous power-recycling schemes enable the failed postselection photons to be repeatedly selected, thus overcoming the inefficient postselection and increasing the precision of detection. In this study, we focus on the polarization-based weak value angular-velocity measurement and introduce three cyclic methods to enhance the accuracy of detecting time shifts in a Gaussian beam: power-recycling, signal-recycling, and dual-recycling schemes. By incorporating one or two partially transmitting mirrors into the system, both the power and the signal-to-noise ratio of the detected light are substantially enhanced. Compared to nonpolarization schemes, polarization-based approaches offer several advantages, including lower optical loss, unique cyclic directions, and a wider optimal region. These features effectively reduce crosstalk among different light paths and theoretically eliminate the walk-off effect, thus yielding improvements in both theoretical performance and application.

DOI: [10.1103/PhysRevA.109.042602](https://doi.org/10.1103/PhysRevA.109.042602)**I. INTRODUCTION**

Since first introduced by Aharonov, Albert, and Vaidman in Ref. [1], weak measurement has shown its numerous potentials in various precise measurements. Unlike the classical (or strong) measurements set forth by von Neumann [2], weak measurement involves a significantly weak coupling between the probe and the system, permitting a small change of coupling parameter to be converted into a large change in a meter variable [1,3]. Consequently, it can be used to reconsider some interesting quantum phenomena such as Hardy's paradox [4–7], the three-box problem [8–10], and quantum Cheshire cats [11–15]. By appropriately preparing pre- and postselected states, weak measurement enables the determination of a “weak value” that encapsulates information regarding the weak interaction process. Generally denoted as  $A_w = \langle f|\hat{A}|i\rangle/\langle f|i\rangle$ , where  $|i\rangle$  and  $|f\rangle$  are the pre- and postselected states, respectively, and  $\hat{A}$  represents the measured observable. Notably, due to the presence of  $\langle f|i\rangle$  in the denominator,  $A_w$  can be very large if  $|i\rangle$  and  $|f\rangle$  are nearly orthogonal. Thus, it has the potential to detect many small physical effects such as the spin Hall effect [16–18], Goos-Hänchen shift [19,20], beam deflection [21], velocity [22], phase shift [23,24], temperature [25], angular-velocity [26–28], and resonance [29], to name a few.

Theoretical analysis has pointed out that weak measurement can outperform the conventional measurement in the presence of detector saturation and pixel noise [30]. Besides, it has been proven that weak measurement can suppress technique noise in some circumstances [16,31] and can

even yield several orders of magnitude improvement over conventional measurements through imaginary weak value measurements [23,32–34]. Furthermore, some reports even proposed Heisenberg-scaling precision postselection measurement using coherent states and photon-counting detection [35–37], which challenges the necessity of entanglement in quantum-enhanced precision. Conversely, negative discussions have primarily centered around the significant loss of photons due to low successful postselection probabilities, resulting in a considerable reduction in the attainable Fisher information [34,35,38,39]. This delicate balance has sparked controversial debates in previous literature [35,38,39]. To address this issue, recycling techniques have been proposed as they are highly compatible with weak measurement and offer the potential to optimize the prevalent disadvantage of diminished Fisher information resulting from low postselection probabilities. At present, three types of weak-value-based recycling techniques have been proposed: power recycling, signal recycling, and dual recycling. The power-recycling technique [40–44], proposed by introducing a partially transmitting mirror (PTM) at the bright port of an interferometer, offers an approach for reusing failed postselection photons. Under ideal conditions, this technique enables the detection of all input light, thus maximizing the efficiency of the system. The similar conclusion is obtained for the signal-recycling weak measurement [45], which works by placing the PTM at the dark port of the interferometer. Furthermore, these power-recycling and signal-recycling techniques can be combined within a dual-recycling scheme to achieve an improved optimal region [46–49].

The previous dual-recycled interferometric weak-value-amplification (WWA) setup obtains large precision improvement while sacrificing some of the WWA effect of pointer due

<sup>\*</sup>qlwu@ccnu.edu.cn

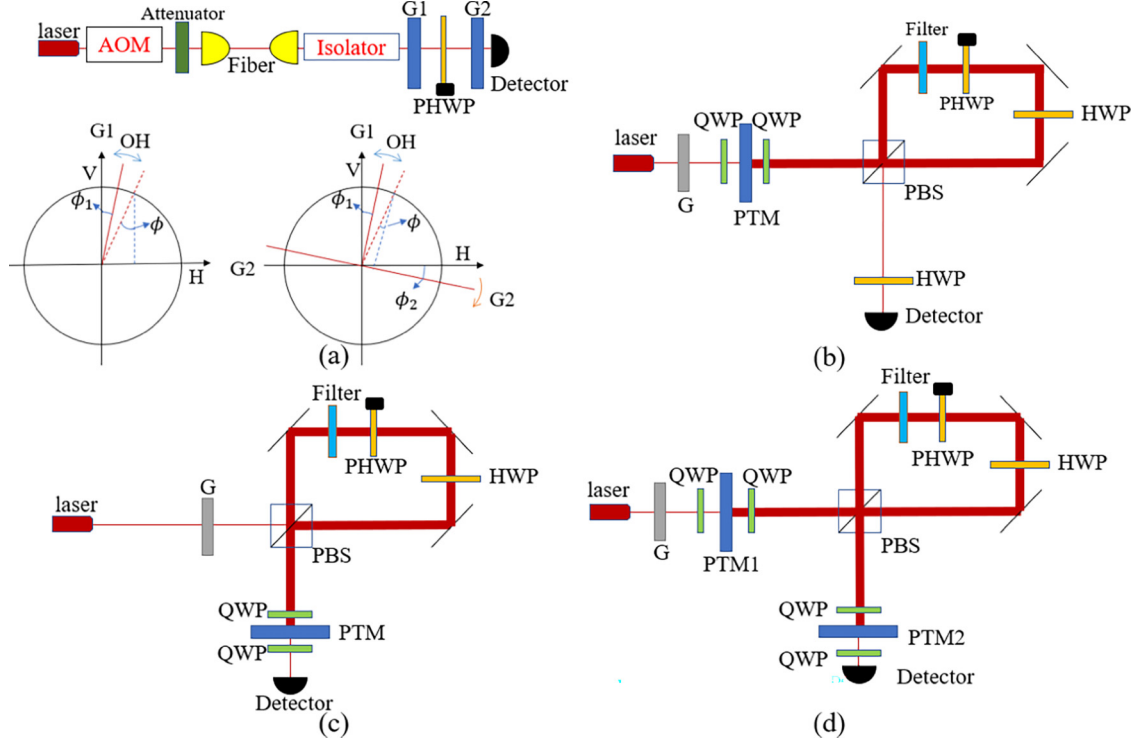


FIG. 1. (a) Schematic of weak-value-based angular-velocity measurement. A laser wave is generated by an acoustic optical modulator (AOM) and enters a polarization-dependent angular velocity measurement system consisting of two Glan prisms (G1 and G2) and the PHWP. The small angular velocity  $\omega$  is induced by the PHWP and finally measured by the detector. The two subfigures below show the different orientations of the optical axis of the Glan prisms and the HWP. (b) The power-recycling scheme. The PBS, which distinguishes the polarization between H and V, is combined with the PTM to reuse the failed postselection photons repeatedly. Two QWPs near the PTM provide the initial polarization and rotate the polarization direction of cyclic light back to V. The filter in front of the PHWP refreshes the beam profile on each pass. The HWP rotates the polarization of light by  $\pi/2$ . (c) The signal-recycling scheme. The PTM at the output port is combined with the WWA system to form a signal-recycling cavity, thus improving the detected signal. (d) The dual-recycling scheme. Combining the power- and signal-recycling PTMs into one scheme further enhances the precision of detection. QWP, quarter-wave plate; HWP, half-wave plate; PBS, polarization beam-splitter; PHWP, piezo-driven half-wave plate; PTM, partially transmitting mirror; H, horizontal; V, vertical; OH, the optical axis of the HWP.

to the walk-off effect. In addition, the intricate path of cyclic photons within the interferometer gives rise to inevitable crosstalk, thereby increasing system loss. To address these challenges, we propose a cyclic scheme for polarization-based weak value amplification, building upon the angular-velocity measurement framework presented in Ref. [50]. In contrast to the nonpolarization cyclic schemes, we substitute the polarization beam splitter (PBS) for the beam splitter (BS). This modification simplifies the light path to be exclusively clockwise  $\odot$  and reduces the optical loss. Moreover, the unidirectional cyclic paths permit a filter to refresh all cyclic photons prior to their final weak interaction, eliminating the walk-off effect.

## II. STANDARD WWA SETUP

We first review the standard WWA setup for angular-velocity measurement in Ref. [50]. As shown in Fig. 1(a), a non-Fourier limit Gaussian pulse  $I_0(t) = (N^2/2\pi\tau^2)^{1/2} \exp(-t^2/2\tau^2)$ , where  $N$  is the number of photons and  $\tau$  is the length of pulse, is sent to a polarization-dependent system. The first Glan prism (G1) combined with the half-wave plate (HWP) provides the

preselected state and the second Glan prism (G2) provides the postselection. In this system, the optical axis of G1 is vertical and the angle between G1 and HWP is  $\phi_1$ . The Gaussian pulse acts as a probe, and the weak interaction is induced by the piezo-driven half-wave plate (PHWP) with an angular velocity,  $\omega$ . After the interaction, the joint state becomes

$$\begin{aligned} |\Psi\rangle &= [\sin(2\phi_1 + 2\omega t)|H\rangle + \cos(2\phi_1 + 2\omega t)|V\rangle] \\ &\times \left(\frac{N^2}{2\pi\tau^2}\right)^{\frac{1}{4}} e^{-\frac{t^2}{4\tau^2}}|t\rangle \\ &= \frac{i}{\sqrt{2}}[e^{-2i(\phi_1 + \omega t)}|R\rangle - e^{2i(\phi_1 + \omega t)}|L\rangle]|\varphi_0\rangle, \end{aligned} \quad (1)$$

where we use the circularly polarized states  $|R\rangle = \frac{1}{\sqrt{2}}(|H\rangle - i|V\rangle)$  and  $|L\rangle = \frac{1}{\sqrt{2}}(|H\rangle + i|V\rangle)$  as basis system states, and we use  $|\varphi_0\rangle$  to express the initial state of probe  $|\varphi_0\rangle = \sqrt{I_0(t)}|t\rangle = (N^2/2\pi\tau^2)^{1/4} \exp(-t^2/4\tau^2)|t\rangle$ . Compared with the initial joint state (after the G1)  $|\Psi_0\rangle = |V\rangle|\varphi_0\rangle = \frac{i}{\sqrt{2}}(|R\rangle - |L\rangle)|\varphi_0\rangle$ , the PHWP here introduces a  $(4\omega t + 4\phi_1)$  phase shift between the left and right circularly polarized components of light, including a  $4\omega$  frequency shift induced by the

weak interaction. Thus, we use  $\hat{U}_w = \exp(i2\omega t\hat{A})$ , where  $\omega$  is the angular velocity by rotating the HWP and  $\hat{A}$  is a Hermitian operator  $\hat{A} = |L\rangle\langle L| - |R\rangle\langle R|$ , to express the weak interaction and we use  $\hat{U}_\phi = \exp(i2\phi_1\hat{A})$  to represent the polarization rotation  $\phi_1$  produced by the PHWP. The preselected state of the system is  $|\psi_{\text{pre}}\rangle = \hat{U}_\phi|V\rangle = \frac{i}{\sqrt{2}}[\exp(-i2\phi_1)|R\rangle - \exp(i2\phi_1)|L\rangle]$  and the postselected state is given by the second Glan prism (G2),  $|\psi_{\text{pos}}\rangle = \cos\phi_2|H\rangle - \sin\phi_2|V\rangle = \frac{i}{\sqrt{2}}[\exp(-i2\phi_2)|R\rangle + \exp(i2\phi_2)|L\rangle]$ , where the initial optical axis of the G2 is horizontal and  $\phi_2$  is the angle of rotation [see Fig. 1(a)]. Therefore, the intensity of detected light is

$$I_d(t) = |\langle\psi_{\text{pos}}|\hat{U}_w|\psi_{\text{pre}}\rangle|\varphi_0\rangle|^2 \approx \frac{N}{\sqrt{2\pi\tau^2}} \sin^2\phi \exp\left[-\frac{1}{2\tau^2}\left(t - \frac{4\omega\tau^2}{\phi}\right)^2\right], \quad (2)$$

where we introduce the angle  $\phi = 2\phi_1 - \phi_2$  and assume  $2\omega\tau \ll \phi \ll 1$ . The corresponding weak value is given by  $A_w = \langle\psi_{\text{pos}}|\hat{A}|\psi_{\text{pre}}\rangle/\langle\psi_{\text{pos}}|\psi_{\text{pre}}\rangle \approx -i/\phi$ . Compared with the incident light, the time shift induced by the PHWP is  $\delta t = \frac{4\omega\tau^2}{\phi} = 4\omega\tau^2|A_w|$ , which is related to the weak value. Based on Fisher information (FI) theory [51,52], the FI of  $\delta t$  is obtained from the detected light  $I_d(t)$ ,

$$\mathcal{F}(\delta t) = \int dt I_d(t) \left| \frac{d}{d\delta t} \ln I_d(t) \right|^2 \approx \frac{N\phi^2}{\tau^2}. \quad (3)$$

So the minimum uncertainty of time shift determined by the Cramér-Rao bound (CRB) satisfies

$$\Delta(\delta t) = \frac{1}{\sqrt{\mathcal{F}(\delta t)}} = \frac{\tau}{\phi\sqrt{N}}. \quad (4)$$

Thus, the minimum uncertainty of angular velocity is

$$\Delta\omega = \frac{\phi}{4\tau^2} \Delta(\delta t) \approx \frac{1}{4\sqrt{N}\tau}. \quad (5)$$

Therefore, the corresponding SNR is given by

$$\text{SNR} = \frac{\omega}{(\Delta\omega)} = 4\omega\tau\sqrt{N} = \frac{\sqrt{N}\phi}{\tau} \delta t. \quad (6)$$

### III. RECYCLING TECHNIQUE

The methodologies of recycling techniques refer to Refs. [40,49], where the improvement of precision is originated from the increasing of weak-value-related photons being detected. The main difference in this method is that it effectively eliminates the opposite traverse shift of the recycling profile by utilizing a filter in a manner made possible by the use of a PBS. This PBS adjusts the optical path within the recycling loop, thereby mitigating the walk-off effect. In addition, the Gaussian light here is modulated in the time domain as opposed to the traditional  $x$  domain. Such arrangement induces a  $\omega$ -related time shift, which enables higher-precision detection. These changes distinguish this model from previous works.

#### A. Power recycling

The power-recycled weak value setup is shown in Fig. 1(b). The initial state  $|V\rangle$  is provided by the Glan prism (G) and two QWPs, and we use the combination ‘‘HWP1 PBS HWP2’’ to replace the G2 for the postselection. The PTM, whose reflection and transmission coefficients are  $r$  and  $p$  ( $r^2 + p^2 = 1$ ), is placed between two QWPs, thus reflecting the failed postselected light while rotating the light polarization to  $|V\rangle$ . Here we define two orthogonal states  $|\psi_1\rangle$  and  $|\psi_2\rangle$  to represent the input and output system states, where  $|\psi_1\rangle = |V\rangle = \frac{i}{\sqrt{2}}(|R\rangle - |L\rangle)$  and  $|\psi_2\rangle = |H\rangle = \frac{1}{\sqrt{2}}(|R\rangle + |L\rangle)$ . Postselected by the input and output ends, the meter states become  $|\varphi_{\text{ref}}\rangle = \langle V|\hat{U}_w\hat{U}_\phi|V\rangle|\varphi_0\rangle$  and  $|\varphi_{\text{out}}\rangle = \langle H|\hat{U}_w\hat{U}_\phi|V\rangle|\varphi_0\rangle$ , respectively. This produces two measurement operators  $M_{11} = \langle\psi_1|\hat{U}_w\hat{U}_\phi|\psi_1\rangle = \cos(\phi + 2\omega t)$  and  $M_{12} = \langle\psi_2|\hat{U}_w\hat{U}_\phi|\psi_1\rangle = \sin(\phi + 2\omega t)$ . We introduce the nonunitary operator  $\hat{L} = \sqrt{1-\gamma}$ , where  $\gamma$  is the single-pass power loss, to express the loss of optical imperfection in one return. Assuming the length of one traversal is  $l_{\text{cav}}$ , the pulse transition time of per traversal is given by  $t_{\text{cav}} = 2l_{\text{cav}}/c$ . Generally, both the measurement operators and the meter state are related to the number of traversals  $n$ . For example,  $M_{11}$  should be written as  $M_{11}^n = \cos[\phi + 2\omega(t - nt_{\text{cav}})]$ . Fang *et al.* [44] proved that this change is small and only induces a constant delay, which can be eliminated. Therefore, with the resonance cavity, the amplitude of the detected signal is given by the sum of amplitudes from all traversal numbers,

$$|\varphi_p\rangle = pM_{12} \sum_{n=0}^{\infty} (rLM_{11})^n |\varphi_0\rangle. \quad (7)$$

It is a summation of the convergence series so that there is a maximum value of  $n$ , denoted by  $n_{\text{max}}$ . Therefore, the formula above can be simplified as

$$|\varphi_p\rangle = pM_{12} \sum_{n=0}^{n_{\text{max}}} (rLM_{11})^n |\varphi_0\rangle \approx \left(\frac{N^2}{2\pi\tau^2}\right)^{\frac{1}{4}} \exp\left(-\frac{t^2}{4\tau^2}\right) \frac{p \sin(\phi + 2\omega t)}{1 - rL \cos(\phi + 2\omega t)} |t\rangle. \quad (8)$$

Next, we do a Taylor expansion on the function  $f(t) = p \sin(\phi + 2\omega t)/[1 - rL \cos(\phi + 2\omega t)]$  and make the approximation  $f(t) \approx f(0) + t f'(0) \approx \exp[-f'(0)t/f(0)]$ . Then the amplitude of the detected state is

$$\langle t|\varphi_p\rangle \approx A \left(\frac{N^2}{2\pi\tau^2}\right)^{\frac{1}{4}} \sin^2(\phi + 2\omega t) \exp\left[-\frac{(t - \delta t_p)^2}{4\tau^2}\right], \quad (9)$$

where

$$A = \frac{p}{1 - r\sqrt{1-\gamma} \cos 2\phi} \quad (10)$$

and

$$\delta t_p = \frac{2\omega\tau^2(\cos\phi - r\sqrt{1-\gamma})}{\sin\phi(1 - r\sqrt{1-\gamma} \cos 2\phi)}. \quad (11)$$

Due to the walk-off effect, the time shift changes from  $\delta t$  to  $\delta t_p$ . But if placing a filter in front of the PHWP, each

time being reflected by the PTM, the light passes through the filter and is projected into  $|\varphi_0\rangle$ . This leaves the prefilter state as  $|\varphi'\rangle_{\text{pow}} = M_{11}|\varphi_0\rangle/\sqrt{|M_{11}\varphi_0|^2}$ . Thus, the probability of surviving the filter is

$$p_f = |\langle\varphi_0|\varphi'\rangle|^2 = \frac{\cos^2\phi}{\sinh 4\omega^2\tau^2 + \cos^2\phi e^{-4\omega^2\tau^2}} \approx 1 - \phi^2(4\omega^2\tau^2) - (4\omega^2\tau^2)^2/2 + \dots, \quad (12)$$

where we make the approximation in the weak value range,  $2\omega\tau \ll \phi \ll 1$ . In this way, the time shift is refreshed every cycle, eliminating the walk-off effect while adding a minimum “filter” loss of  $\gamma_{\min} \approx 4\omega^2\tau^2\phi^2$  to the system [40]. Therefore, the power of the detected signal is given by

$$I_{\text{pow}} \approx \left(\frac{N^2}{2\pi\tau^2}\right)^{\frac{1}{2}} A^2 \sin^2(\phi + 2\omega t) \exp\left[-\frac{(t - \delta t)^2}{2\tau^2}\right]. \quad (13)$$

Similar to the calculation in Eqs. (3)–(6), the corresponding minimum uncertainty determined by the Cramér-Rao bound is

$$\Delta\omega_p \approx \frac{1}{4A\sqrt{N}\tau}. \quad (14)$$

So the corresponding SNR is

$$\text{SNR}_{\text{pow}} \approx A \frac{\sqrt{N}\phi}{\tau} \delta t, \quad (15)$$

which is  $A$  times the SNR of standard weak measurement.

### B. Signal recycling

Similar methods can be used in the signal-recycled scheme. As shown in Fig. 1(c), the optical axis of the Glan prism is vertical, providing the input state  $|V\rangle$ . The postselection is provided by the combination HWP PBS QWPs. The PTM is placed between the two QWPs to reuse the output signal. This postselection processes provide two measurement operators:  $M_{12} = \langle\psi_2|\hat{U}_w\hat{U}_\phi|\psi_1\rangle = \sin(\phi + 2\omega t)$  and  $M_{22} = \langle\psi_2|\hat{U}_w\hat{U}_\phi|\psi_2\rangle = \cos(\phi + 2\omega t)$ . In this signal-recycled cavity, the amplitude of the detected signal is given by

$$|\varphi_s\rangle = pM_{12} \sum_{n=0}^{n_{\max}} (rLM_{22})^n |\varphi_0\rangle \approx \left(\frac{N^2}{2\pi\tau^2}\right)^{\frac{1}{4}} \exp\left(-\frac{t^2}{4\tau^2}\right) \frac{p \sin(\phi + 2\omega t)}{1 - rL \cos(\phi + 2\omega t)} |t\rangle, \quad (16)$$

which is equivalent to  $|\varphi_d\rangle_{\text{pow}}$ , indicating that power- and signal-recycling hold equal significance in weak-value-based power improvement. Different from previous interferometric signal-recycling schemes, the only “clockwise” path permits all cyclic photons to be refreshed prior to the last weak interaction. With the filter, the prefilter state is  $|\varphi'\rangle_{\text{sig}} = M_{22}|\varphi_0\rangle/\sqrt{|M_{22}\varphi_0|^2}$ , which is also equal to  $|\varphi'\rangle_{\text{pow}}$ . Thus, the same conclusion can be obtained when considering the calculation of detected power and SNR, where  $I_{\text{sig}} = I_{\text{pow}}$  and  $\text{SNR}_{\text{sig}} = \text{SNR}_{\text{pow}}$ .

### C. Dual recycling

The dual-recycled WWA scheme is shown in Fig. 1(d), where the Glan prism together with two QWPs provide the input state  $|\psi_1\rangle$  and the output state  $|\psi_2\rangle$  is provided by the combination HWP PBS QWPs. In this recycling process, all possible forms of postselections are available so that the measurement operator of per traversal can be any of  $M_{11}$ ,  $M_{12}$ ,  $M_{21}$ , and  $M_{22}$ . Similarly, the filter in front of the PHWP projects the meter state into  $|\varphi_0\rangle$ , thus eliminating the walk-off effect and maintaining the large point shift associated with the WVA. This also results in a minimum optical loss of  $\gamma_{\min} \approx 4\omega^2\tau^2\phi^2$ , which can be ignored in the weak value range  $2\omega\tau \ll \phi \ll 1$ . For simple calculation, we assume the parameters of PTMs are the same and introduce the measurement matrix

$$U = \begin{bmatrix} M_{11} & M_{12} \\ M_{21} & M_{22} \end{bmatrix} = \begin{bmatrix} \cos(\phi + 2\omega t) & \sin(\phi + 2\omega t) \\ -\sin(\phi + 2\omega t) & \cos(\phi + 2\omega t) \end{bmatrix}, \quad (17)$$

which is formed by four measurement operators and arranged in the order corresponding to the subscripts.  $(U^n)_{12}$  represents the physical process that the incident light travels through the dual-recycling cavity  $n$  times and finally reaches the detector. Therefore, the steady-state amplitude detected by the meter is given by the sum of the amplitudes of all traversal numbers:

$$\begin{aligned} \langle t|\varphi_d\rangle &= p \sum_{n=0}^{n_{\max}} (\sqrt{1-\gamma})^{n+1} (U^{n+1})_{12} p \langle\alpha|\varphi_0\rangle \\ &\approx p^2 \left(\frac{N^2}{2\pi\tau^2}\right)^{\frac{1}{4}} \exp\left(-\frac{t^2}{4\tau^2}\right) \hat{L}\left(\frac{U}{I - r\sqrt{1-\gamma}U}\right)_{12} \\ &= -\frac{p^2 \left(\frac{N^2}{2\pi\tau^2}\right)^{\frac{1}{4}} \exp\left(-\frac{t^2}{4\tau^2}\right) \sqrt{1-\gamma} \sin(\phi + 2\omega t)}{1 + (1-\gamma)r^2 - 2\sqrt{1-\gamma}r \cos(\phi + 2\omega t)} \\ &\approx -\frac{p^2 \left(\frac{N^2}{2\pi\tau^2}\right)^{\frac{1}{4}} \exp\left(-\frac{t^2}{4\tau^2}\right) \sqrt{1-\gamma} \sin(\phi + 2\omega t)}{1 + (1-\gamma)r^2 - 2\sqrt{1-\gamma}r \cos\phi}, \end{aligned} \quad (18)$$

where the last approximation is taken with the minimum filter loss  $\gamma_{\min} \approx 4\omega^2\tau^2\phi^2$ . In this way, the intensity of the detected signal is given by

$$I_{\text{dua}} \approx \left(\frac{N^2}{2\pi\tau^2}\right)^{\frac{1}{2}} B^2 \sin^2(\phi + 2\omega t) \exp\left[-\frac{(t - \delta t)^2}{2\tau^2}\right], \quad (19)$$

where

$$B = \frac{p^2}{1 + (1-\gamma)r^2 - 2\sqrt{1-\gamma}r \cos\phi}. \quad (20)$$

Thus, the corresponding SNR is

$$\text{SNR}_{\text{dua}} \approx B \frac{\sqrt{N}\phi}{\tau} \delta t. \quad (21)$$

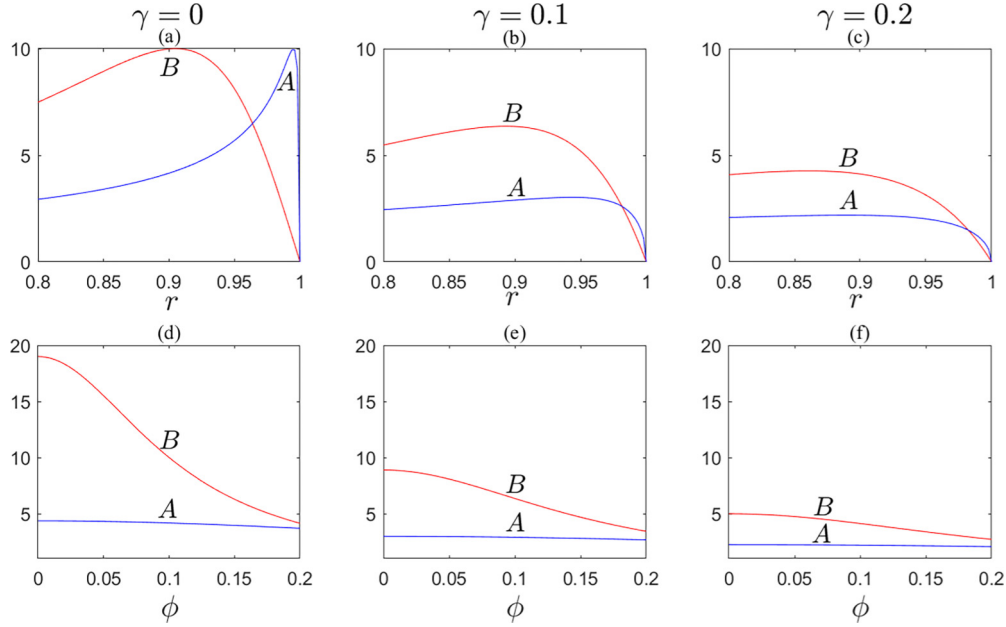


FIG. 2. Comparison of power-, signal- and dual-recycling schemes. Panels (a), (b), and (c) correspond to the cases of  $A$  and  $B$  varying with  $r$  under different values of  $\gamma$ : 0, 0.1, and 0.2, where  $\phi = 0.1$ . In panels (d), (e), and (f), we assume  $r = 0.9$  and plot  $A$  and  $B$  varying with  $\phi$  under  $\gamma = 0, 0.1$ , and  $0.2$ , respectively.  $A$  and  $B$  are the improvement factor of power (or signal) and dual recycling schemes,  $r$  is the reflection coefficient of PTM, and  $\gamma$  is the optical loss.

#### IV. COMPARISON

Here, we define  $A$  and  $B$  as the improvement factors of power (or signal) and dual recycling, respectively. It is clear that the power-, signal-, and dual-recycling schemes improve the SNR of standard WWA setup  $A$ ,  $A$ , and  $B$  times, respectively.  $A^2$  and  $B^2$  also correspond to the improvement of the detected power. Therefore, as shown in Fig. 2, we plot  $A$  and  $B$  varying with  $r$  [Figs. 2(a), 2(b), and 2(c)] or  $\phi$  [Figs. 2(d), 2(e), and 2(f)] under different values of loss  $\gamma = 0, 0.1$ , and  $0.2$ , which correspond to ideal, low, and regular loss, respectively.

As expected, the accuracy of both recycling techniques can easily exceed the corresponding standard scheme's shot noise limit, which is proportionally scaled to 1 in Figs. 2 and 3. The similar conclusions exit in Refs. [41–43,49]. However, we have to declare that it cannot beat the standard quantum limit (SQL) since the improvement originates from the increasing of detected photons  $N\phi^2 \rightarrow B^2N\phi^2$ . Different cyclic schemes only stretch the standard quantum limit to varying degrees. In addition, both  $A$  and  $B$  can reach the maximum value  $1/\phi = 10$ , as shown in Figs. 2(a), 2(b), and 2(c), where the SNR itself is amplified by the large weak value factor. However, the peak of  $A$  decreases faster than that of  $B$ , corresponding to a larger limitation to the improvement of detecting. Therefore, the dual-recycling cavity has tolerance for a wider range of  $r$  and  $\gamma$ , which applies to more circumstances. In Figs. 2(d), 2(e), and 2(f), we set  $r = 0.9$ , a common parameter of the PTM, and draw the curves of  $A$  and  $B$  varying with  $\phi$  where  $\phi \in [0.01, 0.2]$ . We can see that the improvement factor of dual recycling is larger in most weak value ranges, thus outperforming the power or signal recycling.

In the previous dual-recycled interference-based WWA system [49], the amplification effect of pointer is reduced by the walk-off effect, leading to a limitation of the precision

gain. From Eqs. (25) and (26) in Ref. [49], without a filter, the improvement factor  $B$  changes to  $B_{\text{non}}$ :

$$B_{\text{non}} = \xi \frac{p^2}{1 + (1 - \gamma)r^2 - 2\sqrt{1 - \gamma}r \cos \phi}, \quad (22)$$

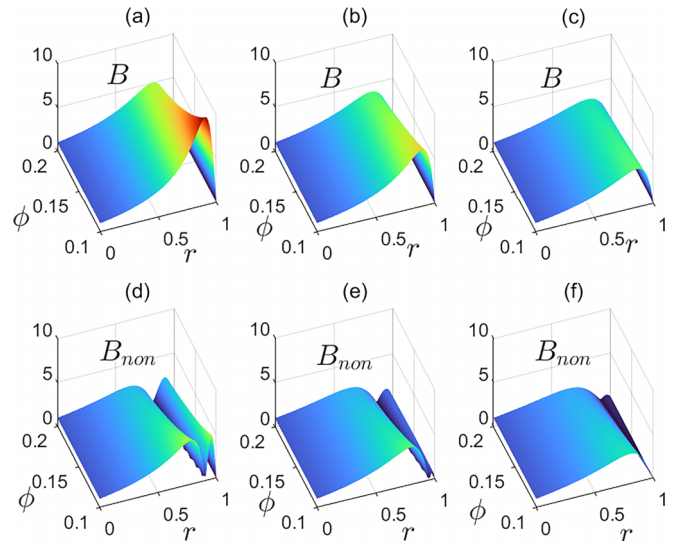


FIG. 3. Comparison of polarization-based and interferometric dual-recycling schemes. Panels (a), (b), and (c) correspond to the case of  $B$  varying with  $r$  and  $\phi$  under different values of  $\gamma$ : 0, 0.1, and 0.2 in three dimensions, respectively. Panels (d), (e), and (f) represent that  $B_{\text{non}}$  varies with  $r$  and  $\phi$  under different values of  $\gamma$ : 0, 0.1 and 0.2 in three dimensions.  $B$  and  $B_{\text{non}}$  are the improvement factors of polarization-based and nonpolarization dual-recycling schemes,  $r$  is the reflection coefficient of PTM,  $\phi$  is the postselected angle, and  $\gamma$  is the optical loss.

where

$$\xi = \phi \frac{\cos \phi [1 + r^2(1 - \gamma)] - 2r\sqrt{1 - \gamma}}{\sin \phi [1 + r^2(1 - \gamma) - 2r\sqrt{1 - \gamma} \cos \phi]}. \quad (23)$$

Due to the proper use of the filter, a minimum filter loss replaces the original performance reduction in the polarization-based dual-recycling scheme. For clear comparison, in Fig. 3, we similarly set  $\phi = 0.1$  and plot  $B$  and  $B_{\text{non}}$  varying with  $r$  and  $\phi$  under different losses. The polarization-based scheme has obvious improvement and the gaps between  $B_{\text{non}}$  and  $B$  decrease as the loss increases. This is established on the assumption that both systems experience the same loss  $\gamma$ . Actually, replacing the BS with the PBS can effectively reduce optical loss. The probability of photons surviving the PBS ( $\geq 95\%$ ) is known to be larger than that of the BS ( $\geq 90\%$ ). In addition, the PBS simplifies the propagation paths of cyclic photons, which reduces the crosstalk among photons. All these reasons make this polarization-based scheme advantageous in both theoretical performance and experimental application.

## V. CONCLUSION

In summary, we have proposed three polarization-based cyclic weak measurement schemes based on the angular-velocity weak measurement setup. By integrating one or two PTMs into the system to establish a resonant cavity, all incident light can be detected in principle. In our analysis, these polarization-based schemes can outperform the previous interferometric schemes due to their lower theoretical loss and improved cyclic paths. This optimized cyclic path effectively eliminates the walk-off effect, a significant challenge in previous signal-recycling and dual-recycling schemes. Notably, among the proposed schemes, the polarization-based dual-recycling scheme demonstrates the widest optimal region.

The application of these cyclic modes is not limited to our specific experimental setup but can be extended to various WVA realizations. This is due to the inherent presence of postselection in all weak value setups. In addition, postselection has been proven to improve the information-cost rate, and negative quasiprobabilities enable postselected experiments to outperform optimal postselection-free experiments [53]. The combination of recycling and negative quasiprobabilities represents a different and meaningful approach. Moreover, leveraging quantum resources allows for precision enhancement beyond the standard quantum limit [54–56], providing a predictable pathway towards further augmenting the performance of weak-value-based metrology.

## ACKNOWLEDGMENT

This work was supported by the National Natural Science Foundation of China (Grant No. 61875067).

## APPENDIX A: FISHER INFORMATION ANALYSIS OF CONVENTIONAL MEASUREMENT

Consider a system prepared in  $|R\rangle$ , one of the basis system states. After the weak interaction, the parameter  $\omega$  is encoded in the meter state as

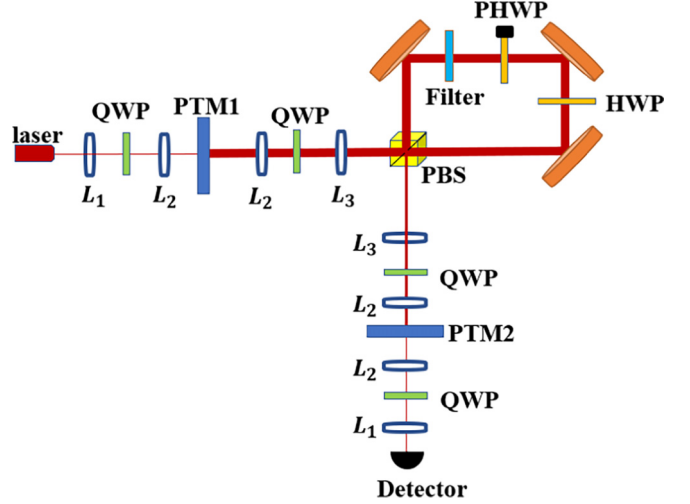


FIG. 4. Optical mode matching and cavity length locking. The lenses  $L_1$ ,  $L_2$ , and  $L_3$  with matched focal lengths are set on proper positions to ensure that the place of the waist and self-reproduction of Gaussian beam are at PTM1 and PTM2. QWP, quarter-wave plate; HWP, half-wave plate; PBS, polarization beam splitter; PHWP, piezo-driven half-wave plate; PTM, partially transmitting mirror.

$|\varphi_c\rangle = (N^2/2\pi\tau^2)^{1/4} \exp(-2i\omega t) \exp(-t^2/4\tau^2)|t\rangle$ . Using the quantum Fisher information (QFI) formula

$$\mathcal{QF}(\omega) = 4 \left[ \left( \frac{d\langle\varphi|}{d\omega} \right) \left( \frac{d|\varphi\rangle}{d\omega} \right) - \left| \langle\varphi| \left( \frac{d|\varphi\rangle}{d\omega} \right) \right|^2 \right], \quad (A1)$$

we can easily get the QFI encoded in  $|\varphi_c\rangle$  as

$$\mathcal{QF}_c(\omega) = 16N\tau^2, \quad (A2)$$

which is also the maximum FI over all possible generalized measurements. Thus, the minimum uncertainty of  $\omega$  is

$$\Delta\omega_c = \frac{1}{\sqrt{\mathcal{QF}_c(\omega)}} = \frac{1}{4\sqrt{N}\tau}. \quad (A3)$$

The corresponding SNR is

$$\text{SNR}_c = \frac{\omega}{\Delta\omega_c} = 4\omega\tau\sqrt{N}. \quad (A4)$$

Comparing  $\Delta\omega_c$  and  $\text{SNR}_c$  with  $\Delta\omega$  and  $\text{SNR}$  [Eqs. (5) and (6)], we can get the conclusion that standard weak value measurement cannot offer better metrological precision of detecting the time shift of the Gaussian beam, which is consistent with the analysis in Ref. [35]. Postselection here acts as a concentration of the information about the parameter to be estimated into small collected parts.

However, by comparing Eqs. (A3) and (A4) to Eqs. (14), (15), and (21), it can be seen that recycled weak value measurement can really enhance metrological precision and outperform conventional measurement. Moreover, this enhancement is consistent with the SQL since it comes from an increase in participating photons  $N \rightarrow A^2N$  (or  $B^2N$ ). In this process, the SQL is stretched from  $1/\sqrt{N}$  to  $1/\sqrt{A^2N}$  (or  $1/\sqrt{B^2N}$ ), without being exceeded.

## APPENDIX B: OPTICAL MODE MATCHING AND STABILITY ANALYSIS

Generally, the beam will be a diffracting Gaussian beam with a waist, as opposed to the parallel beam treated above. Therefore, the waist size and positions of the incident Gaussian beam should match those of the resonance cavity itself, forming a stable self-reproduction. Here, we take the most challenging dual-recycling as an example, as illustrated in Fig. 4. Similar to the solutions of Refs. [41,49], several well-designed lenses  $L_1$ ,  $L_2$ , and  $L_3$  are employed to ensure the waists are located at PTM1 and PTM2.

The phase locking of the cavity is also essential since the ambient noise can introduce length offsets in the cavity. In Ref. [41], an error signal extracted from the output light is

used to provide feedback and stabilize the power-recycling cavity using the Pound-Drever-Hall (PDH) method, which is also applicable to the signal-recycling cavity. However, when implementing the dual-recycling cavity with two different lengths, relying solely on an error signal does not provide sufficient information regarding the offsets of the PTMs. A possible approach is to adjust the postselected angle and parameters of the PTMs such that the light reflected towards the laser is largely independent of PTM2, allowing the first PDH system to initially lock the length of PTM1 before using the second PDH system to stabilize the length of PTM2. Alternatively, a custom-designed enclosure with fixed positions for the instruments can simplify the locking operations.

- 
- [1] Y. Aharonov, D. Z. Albert, and L. Vaidman, How the result of a measurement of a component of the spin of a spin-1/2 particle can turn out to be 100, *Phys. Rev. Lett.* **60**, 1351 (1988).
- [2] J. von Neumann, in *Mathematical Foundations of Quantum Mechanics*, edited by N. A. Wheeler (Princeton University, Princeton, NJ, 2018).
- [3] A. M. Steinberg, A light touch, *Nature (London)* **463**, 890 (2010).
- [4] L. Hardy, Quantum mechanics, local realistic theories, and Lorentz-invariant realistic theories, *Phys. Rev. Lett.* **68**, 2981 (1992).
- [5] Y. Aharonov, A. Botero, S. Popescu, B. Reznik, and J. Tollaksen, Revisiting Hardy's paradox: counterfactual statements, real measurements, entanglement and weak values, *Phys. Lett. A* **301**, 130 (2002).
- [6] J. S. Lundeen and A. M. Steinberg, Experimental joint weak measurement on a photon pair as a probe of Hardy's paradox, *Phys. Rev. Lett.* **102**, 020404 (2009).
- [7] K. Yokota, T. Yamamoto, M. Koashi, and N. Imoto, Direct observation of Hardy's paradox by joint weak measurement with an entangled photon pair, *New J. Phys.* **11**, 033011 (2009).
- [8] Y. Aharonov and L. Vaidman, Complete description of a quantum system at a given time, *J. Phys. A: Math. Gen.* **24**, 2315 (1991).
- [9] T. Ravon and L. Vaidman, The three-box paradox revisited, *J. Phys. A: Math. Theor.* **40**, 2873 (2007).
- [10] K. J. Resch, J. S. Lundeen, and A. M. Steinberg, Experimental realization of the quantum box problem, *Phys. Lett. A* **324**, 125 (2004).
- [11] Y. Aharonov, S. Popescu, D. Rohrlich, and P. Skrzypczyk, Quantum Cheshire cats, *New J. Phys.* **15**, 113015 (2013).
- [12] Y. Aharonov, E. Cohen, and S. Popescu, A dynamical quantum Cheshire Cat effect and implications for counterfactual communication, *Nat. Commun.* **12**, 4770 (2021).
- [13] T. Denkmayr, H. Geppert, S. Sponar, H. Lemmel, A. Matzkin, J. Tollaksen, and Y. Hasegawa, Observation of a quantum Cheshire Cat in a matter-wave interferometer experiment, *Nat. Commun.* **5**, 4492 (2014).
- [14] Q. Duprey, S. Kanjilal, U. Sinha, D. Home, and A. Matzkin, The quantum Cheshire cat effect: Theoretical basis and observational implications, *Ann. Phys.* **391**, 1 (2018).
- [15] J. Q. Quach, Dual to the anomalous weak-value effect of photon-polarization separation, *Phys. Rev. A* **100**, 052117 (2019).
- [16] O. Hosten and P. Kwiat, Observation of the spin Hall effect of light via weak measurements, *Science* **319**, 787 (2008).
- [17] X. Zhou, Z. Xiao, H. Luo, and S. Wen, Experimental observation of the spin Hall effect of light on a nanometal film via weak measurements, *Phys. Rev. A* **85**, 043809 (2012).
- [18] X. Bai, Y. Liu, L. Tang, Q. Zang, J. Li, W. Lu, H. Shi, X. Sun, and Y. Lu, Impact of the pitch angle on the spin Hall effect of light weak measurement, *Opt. Express* **28**, 15284 (2020).
- [19] X.-Y. Xu, Y. Kedem, K. Sun, L. Vaidman, C.-F. Li, and G.-C. Guo, Phase estimation with weak measurement using a white light source, *Phys. Rev. Lett.* **111**, 033604 (2013).
- [20] L. Li, Y. Li, Y.-L. Zhang, S. Yu, C.-Y. Lu, N.-L. Liu, J. Zhang, and J.-W. Pan, Phase amplification in optical interferometry with weak measurement, *Phys. Rev. A* **97**, 033851 (2018).
- [21] P. B. Dixon, D. J. Starling, A. N. Jordan, and J. C. Howell, Ultrasensitive beam deflection measurement via interferometric weak value amplification, *Phys. Rev. Lett.* **102**, 173601 (2009).
- [22] G. I. Viza, J. Martínez-Rincón, G. A. Howland, H. Frostig, I. Shomroni, B. Dayan, and J. C. Howell, Weak-values technique for velocity measurements, *Opt. Lett.* **38**, 2949 (2013).
- [23] N. Brunner and C. Simon, Measuring small longitudinal phase shifts: Weak measurements or standard interferometry? *Phys. Rev. Lett.* **105**, 010405 (2010).
- [24] X. Qiu, L. Xie, X. Liu, L. Luo, Z. Li, Z. Zhang, and J. Du, Precision phase estimation based on weak-value amplification, *Appl. Phys. Lett.* **110**, 071105 (2017).
- [25] H. Li, J.-Z. Huang, Y. Yu, Y. Li, C. Fang, and G. Zeng, High-precision temperature measurement based on weak measurement using nematic liquid crystals, *Appl. Phys. Lett.* **112**, 231901 (2018).
- [26] M. Pfeifer and P. Fischer, Weak value amplified optical activity measurements, *Opt. Express* **19**, 16508 (2011).
- [27] O. S. Magaña-Loaiza, M. Mirhosseini, B. Rodenburg, and R. W. Boyd, Amplification of angular rotations using weak measurements, *Phys. Rev. Lett.* **112**, 200401 (2014).

- [28] B. de Lima Bernardo, S. Azevedo, and A. Rosas, Ultrasmall polarization rotation measurements via weak value amplification, *Phys. Lett. A* **378**, 2029 (2014).
- [29] W. Qu, S. Jin, J. Sun, L. Jiang, J. Wen, and Y. Xiao, Sub-Hertz resonance by weak measurement, *Nat. Commun.* **11**, 1752 (2020).
- [30] J. Harris, R. W. Boyd, and J. S. Lundeen, Weak value amplification can outperform conventional measurement in the presence of detector saturation, *Phys. Rev. Lett.* **118**, 070802 (2017).
- [31] D. J. Starling, P. B. Dixon, A. N. Jordan, and J. C. Howell, Optimizing the signal-to-noise ratio of a beam-deflection measurement with interferometric weak values, *Phys. Rev. A* **80**, 041803(R) (2009).
- [32] A. Feizpour, X. Xing, and A. M. Steinberg, Amplifying single-photon nonlinearity using weak measurements, *Phys. Rev. Lett.* **107**, 133603 (2011).
- [33] Y. Kedem, Using technical noise to increase the signal-to-noise ratio of measurements via imaginary weak values, *Phys. Rev. A* **85**, 060102(R) (2012).
- [34] A. N. Jordan, J. Martínez-Rincón, and J. C. Howell, Technical advantages for weak-value amplification: When less is more, *Phys. Rev. X* **4**, 011031 (2014).
- [35] L. Zhang, A. Datta, and I. A. Walmsley, Precision metrology using weak measurements, *Phys. Rev. Lett.* **114**, 210801 (2015).
- [36] G. Chen, L. Zhang, W.-H. Zhang, X.-X. Peng, L. Xu, Z.-D. Liu, X.-Y. Xu, J.-S. Tang, Y.-N. Sun, D.-Y. He, J.-S. Xu, Z.-Q. Zhou, C.-F. Li, and G.-C. Guo, Achieving Heisenberg-scaling precision with projective measurement on single photons, *Phys. Rev. Lett.* **121**, 060506 (2018).
- [37] Y. Liu, L. Qin, and X.-Q. Li, Fisher information analysis on weak-value-amplification metrology using optical coherent states, *Phys. Rev. A* **106**, 022619 (2022).
- [38] C. Ferrie and J. Combes, Weak value amplification is suboptimal for estimation and detection, *Phys. Rev. Lett.* **112**, 040406 (2014).
- [39] G. C. Knee and E. M. Gauger, When amplification with weak values fails to suppress technical noise, *Phys. Rev. X* **4**, 011032 (2014).
- [40] K. Lyons, J. Dressel, A. N. Jordan, J. C. Howell, and P. G. Kwiat, Power-recycled weak-value-based metrology, *Phys. Rev. Lett.* **114**, 170801 (2015).
- [41] Y.-T. Wang, J.-S. Tang, G. Hu, J. Wang, S. Yu, Z.-Q. Zhou, Z.-D. Cheng, J.-S. Xu, S.-Z. Fang, Q.-L. Wu, C.-F. Li, and G.-C. Guo, Experimental demonstration of higher precision weak-value-based metrology using power recycling, *Phys. Rev. Lett.* **117**, 230801 (2016).
- [42] J. Dressel, K. Lyons, A. N. Jordan, T. M. Graham, and P. G. Kwiat, Strengthening weak-value amplification with recycled photons, *Phys. Rev. A* **88**, 023821 (2013).
- [43] C. Krafczyk, A. N. Jordan, M. E. Goggin, and P. G. Kwiat, Enhanced Weak-value amplification via photon recycling, *Phys. Rev. Lett.* **126**, 220801 (2021).
- [44] S.-Z. Fang, L.-L. Zhu, R.-B. Jin, H.-T. Tan, G.-X. Li, and Q.-L. Wu, Ultrasensitive velocity estimation via cyclic weak measurement, *Opt. Commun.* **460**, 125117 (2020).
- [45] B. J. Meers and K. A. Strain, Wave-front distortion in laser-interferometric gravitational-wave detectors, *Phys. Rev. D* **43**, 3117 (1991).
- [46] K. A. Strain and B. J. Meers, Experimental demonstration of dual recycling for interferometric gravitational-wave detectors, *Phys. Rev. Lett.* **66**, 1391 (1991).
- [47] B. P. Abbott *et al.* (LIGO Scientific Collaboration and Virgo Collaboration), Observation of gravitational waves from a binary black hole merger, *Phys. Rev. Lett.* **116**, 061102 (2016).
- [48] B. P. Abbott *et al.* (LIGO Scientific Collaboration and Virgo Collaboration), GW150914: The advanced LIGO detectors in the era of first discoveries, *Phys. Rev. Lett.* **116**, 131103 (2016).
- [49] Z.-R. Zhong, W.-J. Tan, Y. Chen, and Q.-L. Wu, Dual-recycled interference-based weak value metrology, *Phys. Rev. A* **108**, 032608 (2023).
- [50] S.-Z. Fang, H.-T. Tan, G.-X. Li, and Q.-L. Wu, Weak value amplification for angular velocity measurements, *Appl. Opt.* **60**, 4335 (2021).
- [51] C. M. Care, Probabilistic and statistical aspects of quantum theory: North-Holland series in Statistics and Probability Vol 1, *Phys. Bull.* **34**, 395 (1983).
- [52] C. Helstrom and R. Kennedy, Noncommuting observables in quantum detection and estimation theory, *IEEE Trans. Inf. Theory* **20**, 16 (1974).
- [53] D. R. M. Arvidsson-Shukur, N. Yunger Halpern, H. V. Lepage, C. H. W. Barnes, and S. Lloyd, Quantum advantage in postselected metrology, *Nat. Commun.* **11**, 3775 (2020).
- [54] S. Pang, J. Dressel, and T. A. Brun, Entanglement-assisted weak value amplification, *Phys. Rev. Lett.* **113**, 030401 (2014).
- [55] J.-S. Chen, B.-H. Liu, M.-J. Hu, X.-M. Hu, C.-F. Li, G.-C. Guo, and Y.-S. Zhang, Realization of entanglement-assisted weak-value amplification in a photonic system, *Phys. Rev. A* **99**, 032120 (2019).
- [56] S. Pang and T. A. Brun, Improving the precision of weak measurements by postselection measurement, *Phys. Rev. Lett.* **115**, 120401 (2015).